

# Simulation of waves in fractured media using an extrapolation scheme

Yaping Zhu\* and Roel Snieder, Center for Wave Phenomena, Colorado School of Mines, Golden, CO 80401

## Summary

Equivalent medium theory has been widely used in finite-difference simulation of wave propagation in fractured media by simulating a fracture with a thin low-velocity layer. Here we show how slip-discontinuity can be incorporated into the finite-difference scheme without using the equivalent low-velocity model. We develop an extrapolation scheme for the simulation in which two  $9 \times 9$  well-determined linear systems are designed to guarantee the stability of the extrapolation. Since both systems are time-invariant, extra computation cost for the simulation is negligible. Numerical examples support the validity of this approach.

## Introduction

A common way to model wave propagation in fractures is to use an equivalent medium to represent a fracture (Igel et al., 1997; Coates and Schoenberg, 1995), e.g., a low-velocity layer. Schoenberg (1980) discussed the equivalence between a thin low-velocity layer and an idealized fracture. The underlying assumptions for the equivalence between the low-velocity layer and the fracture are: 1) the thickness of the low-velocity layer should be much smaller than the wavelength; 2) the impedance in the layer should be much smaller than that in the background media. Coates and Schoenberg (1995) discussed finite-difference modeling of faults and fractures based on the equivalent medium when the grid is intersected by the fracture.

The advantage of using an equivalent low-velocity-layer model in finite-difference simulation is that it requires no special treatment of the boundary conditions. However, since it requires the thickness to be much smaller than the wavelength and the impedance in the layer to be much smaller than that in the background media, both grid size and time step need to be small.

In this paper, we discuss finite-difference simulation of wavefield in the fractured media without using the equivalent low-velocity-layer model. We developed an extrapolation scheme which allows us to treat the linear-slip boundary condition directly. It is based on velocity-stress finite-differencing on a staggered-grid (Virieux, 1984; Virieux, 1986), which updates the particle velocities and stresses alternatively at each time step. In our approach, two  $9 \times 9$  linear systems are designed for evaluating the particle velocities and stresses at the fracture interface, one for  $v_x$  and  $\tau_{xz}$  and another for  $v_z$  and  $\tau_{zx}$ . For each time step we update first the particle velocities  $v_x$  and  $v_z$  and the stress component  $\tau_{xx}$  in the same way as in a standard staggered-grid scheme, we then update

the stress components  $\tau_{xz}$  and  $\tau_{zx}$  according to these two  $9 \times 9$  linear systems. We will show that the coefficient matrices in these systems are time-invariant and need to be solved only once at the beginning of the simulation. Hence extra computation cost for simulating the fractures is negligible. Numerical examples support the validity of this approach.

## Extrapolation scheme for simulating fractures

Consider the velocity-stress representation of a 2-D wave equation for the fractured media. A fracture is a non-welded interface across which the tractions are continuous while the displacements are discontinuous. A simple way to describe the displacement discontinuity is the elastic boundary condition, often denoted as the linear-slip interface condition (Schoenberg, 1980; Fan et al., 1996; Schoenberg, 1998; Myer, 1998).

In the presence of a horizontal fracture (in  $x$ -direction), we have

$$\begin{aligned}\frac{\partial v_x}{\partial t} &= \frac{1}{\rho} \left( \frac{\partial \tau_{xx}}{\partial x} + \frac{\partial \tau_{xz}}{\partial z} \right), \\ \frac{\partial v_z}{\partial t} &= \frac{1}{\rho} \left( \frac{\partial \tau_{xz}}{\partial x} + \frac{\partial \tau_{zz}}{\partial z} \right), \\ \frac{\partial \tau_{xx}}{\partial t} &= (\lambda + 2\mu) \frac{\partial v_x}{\partial x} + \lambda \frac{\partial v_z}{\partial z}, \\ \frac{\partial \tau_{zz}}{\partial t} &= \mathcal{K}_z [v_z], \\ \frac{\partial \tau_{xz}}{\partial t} &= \mathcal{K}_x [v_x],\end{aligned}\tag{1}$$

where  $v$  denotes the particle velocity,  $\tau$  denotes the stress, and  $\lambda$  and  $\mu$  are the Lamé parameters. The square brackets here denote the difference between the particle velocities across the fracture interface.  $\mathcal{K}$  is the fracture stiffness, which is an indicator of the strength of the fracture.

In the calculation of the stresses given by expression (1), we extrapolate the particle velocity from neighboring points to the point where the stress needs to be evaluated, as illustrated in Figure 1. We then calculate the difference between the extrapolated particle velocities across the fracture, which accounts for the time derivative of the stress, and finally get the updated stress at that point.

A direct extrapolation of the particle velocity (or the particle displacement) would be a natural way to evaluate the displacement discontinuity at the fracture interface, but it fails when the number of unknowns used in the extrapolation scheme exceeds that of constraints, which causes error in evaluating the stress. Hence further constraints need to be considered. To fully constrain the

## An SEG abstract running header

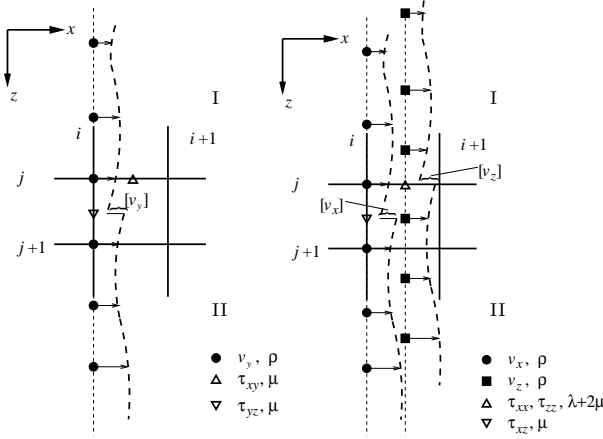


Fig. 1: Staggered grid used in handling the elastic boundary condition, shown in expression (2), in the elastic finite-difference calculations.  $i$  and  $i+1$  denote the index of the nodes on the grid in the  $x$  direction;  $j$  and  $j+1$  denote the index of the nodes on the grid in the  $z$  direction. Thick dashed curves denote the magnitude of the particle velocities, and the square brackets denote the difference between the displacements above and below the fracture. The particle velocities at neighboring points are extrapolated to the point where the stress component needs to be evaluated. Left: modeling the SH-wave where the stress component  $\tau_{yz}$  is calculated based on the difference between the particle displacements, which are the time integral of the difference between the particle velocities,  $[v_y]$ . Right: modeling the P-SV waves where the stress components  $\tau_{xz}$  and  $\tau_{zz}$  are calculated based on the difference between the particle displacements which are the time integrals of the difference between the particle velocities,  $[v_x]$  and  $[v_z]$ , respectively. A polynomial extrapolation technique is used.

extrapolation, we take the constituent relationship into consideration.

For medium I, we use two second-order polynomials to approximate the particle velocities near the fracture. Hence we have

$$\begin{aligned} az_{j-1}^2 + bz_{j-1} + c &= v_{xj-1}, \\ az_j^2 + bz_j + c &= v_{xj}, \\ az_{j+\frac{1}{2}}^2 + bz_{j+\frac{1}{2}} + c &= v_{xj+\frac{1}{2}}^I, \end{aligned} \quad (2)$$

for the particle velocity  $v_x$  and

$$\begin{aligned} a'z_{j-\frac{3}{2}}^2 + b'z_{j-\frac{3}{2}} + c' &= v_{zj-\frac{3}{2}}, \\ a'z_{j-\frac{1}{2}}^2 + b'z_{j-\frac{1}{2}} + c' &= v_{zj-\frac{1}{2}}, \\ a'z_j^2 + b'z_j + c' &= v_{zj}^I, \end{aligned} \quad (3)$$

for the particle velocity  $v_z$ . The stress components  $\tau_{xz}$  and  $\tau_{zz}$  are governed by the following constituent relationship

$$\left(\frac{\partial\tau_{xz}}{\partial t}\right)_{j+\frac{1}{2}} = \mu_{j+\frac{1}{2}}(2az_{j+\frac{1}{2}} + b) + \mu_{j+\frac{1}{2}}\left(\frac{\partial v_z}{\partial x}\right)_{j+\frac{1}{2}},$$

$$\left(\frac{\partial\tau_{zz}}{\partial t}\right)_j = (\lambda_j + 2\mu_j)(2a'z_j + b') + \lambda_j\left(\frac{\partial v_x}{\partial x}\right)_j. \quad (4)$$

where  $a$  through  $c$  and  $a'$  through  $c'$  are coefficients of the above second-order polynomials.

Medium II is treated in the similar way. Re-organizing expressions for both media leads to two  $9 \times 9$  linear systems:

$$\begin{aligned} az_{j-1}^2 + bz_{j-1} + c &= v_{xj-1}, \\ az_j^2 + bz_j + c &= v_{xj}, \\ az_{j+\frac{1}{2}}^2 + bz_{j+\frac{1}{2}} + c &= v_{xj+\frac{1}{2}}^I, \\ dz_{j+1}^2 + ez_{j+1} + f &= v_{xj+1}, \\ dz_{j+2}^2 + ez_{j+2} + f &= v_{xj+2}, \\ dz_{j+\frac{1}{2}}^2 + ez_{j+\frac{1}{2}} + f &= v_{xj+\frac{1}{2}}^{II}, \\ \left(\frac{\partial\hat{\tau}_{xz}}{\partial t}\right)_{j+\frac{1}{2}} &= (2az_{j+\frac{1}{2}} + b) + \left(\frac{\partial v_z}{\partial x}\right)_{j+\frac{1}{2}}, \\ \left(\frac{\partial\hat{\tau}_{xz}}{\partial t}\right)_{j+\frac{1}{2}} &= (2dz_{j+\frac{1}{2}} + e) + \left(\frac{\partial v_z}{\partial x}\right)_{j+\frac{1}{2}}, \\ \left(\frac{\partial\hat{\tau}_{xz}}{\partial t}\right)_{j+\frac{1}{2}} &= \frac{\mathcal{K}_{xj+\frac{1}{2}}}{\mu_{j+\frac{1}{2}}}(v_{xj+\frac{1}{2}}^{II} - v_{xj+\frac{1}{2}}^I), \end{aligned} \quad (5)$$

where the nine unknowns are  $a$  through  $f$ ,  $v_{xj+\frac{1}{2}}^I$ ,  $v_{xj+\frac{1}{2}}^{II}$ , and  $\left(\frac{\partial\hat{\tau}_{xz}}{\partial t}\right)_{j+\frac{1}{2}}$ , and

$$\begin{aligned} a'z_{j-\frac{3}{2}}^2 + b'z_{j-\frac{3}{2}} + c' &= v_{zj-\frac{3}{2}}, \\ a'z_{j-\frac{1}{2}}^2 + b'z_{j-\frac{1}{2}} + c' &= v_{zj-\frac{1}{2}}, \\ a'z_j^2 + b'z_j + c' &= v_{zj}^I, \\ d'z_{j+\frac{1}{2}}^2 + e'z_{j+\frac{1}{2}} + f' &= v_{zj+\frac{1}{2}}, \\ d'z_{j+\frac{3}{2}}^2 + e'z_{j+\frac{3}{2}} + f' &= v_{zj+\frac{3}{2}}, \\ d'z_j^2 + e'z_j + f' &= v_{zj}^{II}, \\ \left(\frac{\partial\hat{\tau}_{zz}}{\partial t}\right)_j &= (2a'z_j + b') + \frac{\lambda_j}{(\lambda_j + 2\mu_j)}\left(\frac{\partial v_x}{\partial x}\right)_j, \\ \left(\frac{\partial\hat{\tau}_{zz}}{\partial t}\right)_j &= (2d'z_j + e') + \frac{\lambda_j}{(\lambda_j + 2\mu_j)}\left(\frac{\partial v_x}{\partial x}\right)_j, \\ \left(\frac{\partial\hat{\tau}_{zz}}{\partial t}\right)_j &= \frac{\mathcal{K}_{zj}}{(\lambda_j + 2\mu_j)}(v_{zj}^{II} - v_{zj}^I). \end{aligned} \quad (6)$$

Here the nine unknowns are  $a'$  through  $f'$ ,  $v_{zj}^I$ ,  $v_{zj}^{II}$ , and  $\left(\frac{\partial\hat{\tau}_{zz}}{\partial t}\right)_j$ . The stress components are normalized by the Lamé parameters:  $\hat{\tau}_{xz} = \frac{\tau_{xz}}{\mu_j}$  and  $\hat{\tau}_{zz} = \frac{\tau_{zz}}{(\lambda + 2\mu)}$ .

Both linear systems are non-singular, which guarantees the stability of the solution of velocities and stresses at the fracture interface. Since coefficients in both linear systems are fully governed by the grid size and normalized medium parameters, both linear systems are time-invariant, which means that we need to solve the matrices

## An SEG abstract running header

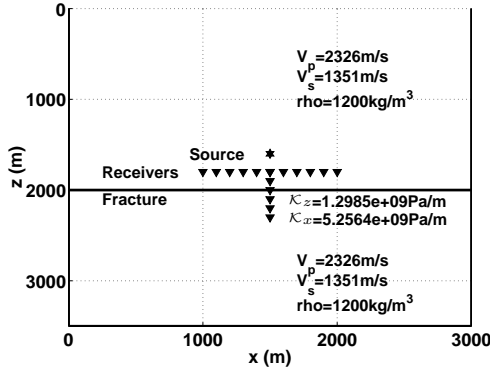


Fig. 2: Geometry of the model with an idealized planar fracture.

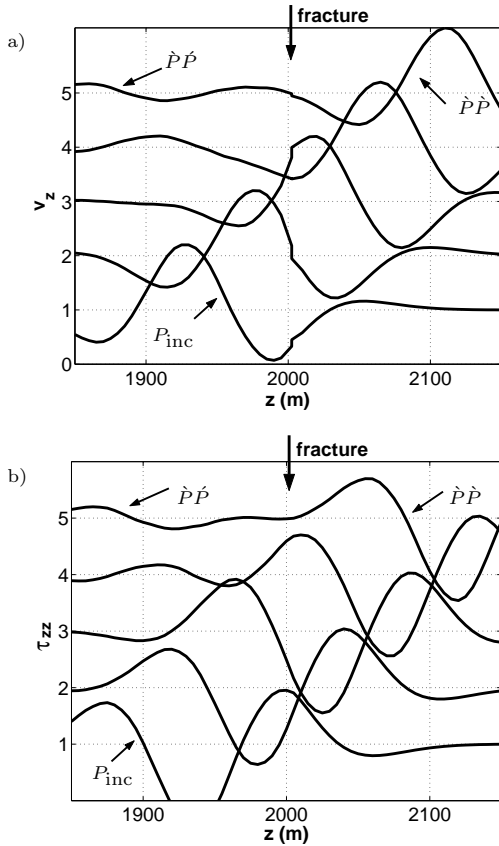


Fig. 3: Different space-time snapshots of a) the normalized vertical component of the particle velocity  $v_z$  and b) the normal stress component  $\tau_{zz}$ , during the wave propagation through a fracture at normal incidence. The difference in time between subsequent plots is 0.02 s. The fracture is located at the depth of 2000 m, and the vertical grid spacing in the simulation is 5 m. A discontinuity is observed for  $v_z$  across the fracture, while  $\tau_{zz}$  is continuous across the fracture.

only once and use them for all the following time steps in the simulation. Thus the extra computation cost for simulating the fractures is negligible, especially for fractures where the fracture stiffnesses and the background medium parameters remain constant.

## Numerical example and verification

To test the validity of the finite-difference code, we consider P-SV waves in a two-layer model with an idealized planar fracture embedded in constant-background media (Figure 2). An idealized planar fracture is placed at a depth of 2000 m. The fracture stiffnesses are set as  $\mathcal{K}_z = 1.2985 \times 10^9$  Pa/m and  $\mathcal{K}_x = 5.2564 \times 10^9$  Pa/m. The grid spacing is 5 m for both  $x$  and  $z$ -direction, the time step is 0.25 ms, and the number of grid points in the test example is  $1201 \times 1401$ . A P-wave was excited from a point source at the position marked by an asterisk. The source wave is a Ricker wavelet with the dominant frequency of 12 Hz. An array of receivers is located at a depth of 1800 m, with horizontal offsets extending from -500 m to 500 m. Another array of receivers is located below the source, with the depth extending from 1800 m to 2200 m to record snapshots of the waves propagating through the fracture. In Igel et al. (2001), the number of points per dominant wavelength is set at 20 in the numerical simulation of fault zones characterized as low-velocity zones. In our numerical test, we recommend that within the fracture region the number of points in the dominant wavelength be set at  $\geq 40$ .

In Figure 3, we show snapshots of the modeled vertical particle velocity  $v_z$  and normal stress  $\tau_{zz}$  across the fracture. The P-wave propagates at normal incidence through the fracture at the depth of 2000 m. The discontinuity is visible for  $v_z$  across the fracture, while  $\tau_{zz}$  is continuous across the fracture. The figure shows how a fracture is modeled as a linear-slip boundary condition.

Figure 4a shows the modeled PP reflected field at normal incidence. Compared to the analytical solution for the PP reflection at normal incidence (Chaisri and Krebs, 2000), the error of the peak amplitude in the numerical simulation is less than 5%. For larger offset, as shown in Figure 4b, the particle polarization for PP and P-SV reflections needs to be considered in order to evaluate the amplitude of PP and P-SV reflections from  $x$ - and  $z$ -component data. Comparison between the numerical and analytic solution also supports the validity of the finite-difference scheme in simulating waves excited by fractures.

## Discussion and conclusions

Using the staggered-grid finite-difference, we developed an extrapolation scheme for simulating wave propagation influenced by fractures described as linear slip boundaries. In the update of the stresses at each time step in the region of fractures, particle velocities are extrapolated from neighboring points to the point where stresses need to

## An SEG abstract running header

be evaluated and the difference between the extrapolated particle velocities across the fracture is calculated to get the time derivative of the stress. To make the extrapolation stable, the constituent relationship is taken as a constraint on the extrapolation.

The extrapolation scheme is valid for media containing a system of fractures or cracks. To make the extrapolation stable for a fracture, other fractures should not be present at neighboring points of this fracture, which requires that the number of grid points between two adjacent fractures be at least four for second-order extrapolation. That explains why in the region of fractures the number of points per dominant wavelength is relatively large, e.g., no less than 40 in our numerical tests.

Note that for fractures, wherever the fracture stiffnesses and the background medium parameters are constant along the fractures, only two  $9 \times 9$  linear systems are required; otherwise different linear systems need to be solved for each grid point on the fracture where either the fracture stiffness or the background medium parameters change. Fortunately, the coefficient matrices in both the linear systems are time-invariant, which means that we need to solve those matrices only once and use them for all the following time steps in the simulation. Thus the extra computation cost for simulating the fractures is negligible.

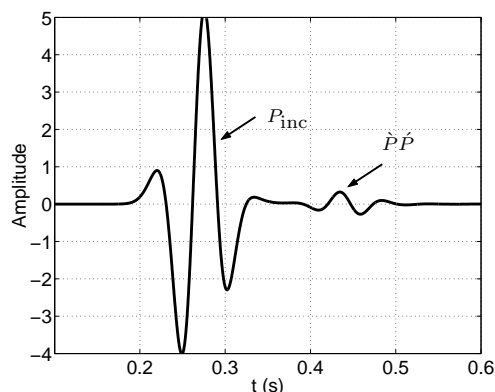
### Acknowledgments

This work was supported by the sponsors of the Consortium Project on Seismic Inverse Methods for Complex Structures at the Center for Wave Phenomena.

### References

- Chaisri, S., and Krebs, E. S., 2000, Exact and approximate formulas for P-SV reflection and transmission coefficients for a nonwelded contact interface: *J. Geophys. Res.*, **105**, 28045–28054.
- Coates, R. T., and Schoenberg, M., 1995, Finite-difference modeling of faults and fractures: *Geophysics*, **60**, 1514–1526.
- Fan, J., Gu, B., Nihei, K. T., Cook, N. G. W., and Myer, L. R., 1996, Experimental and numerical investigation of fracture interface waves: *Rock Mechanics*, Balkema, Rotterdam, 845–851.
- Igel, H., Ben-Zion, Y., and Leary, P. C., 1997, Simulation of SH- and P-SV- wave propagation in fault zones: *Geophys. J. Int.*, **128**, 533–546.
- Igel, H., Jahnke, G., and Ben-Zion, Y., 2001, Numerical simulation of fault zone guided waves: accuracy and 3-D effects: *PAGEOPH*, in press.
- Myer, L., 1998, Seismic wave propagation in fractured rock, *in* Rossmanith, Ed., *Mechanics of jointed and faulted rock*, Balkema, Rotterdam, 29–38.

a) offset=0 m



b) offset=200 m

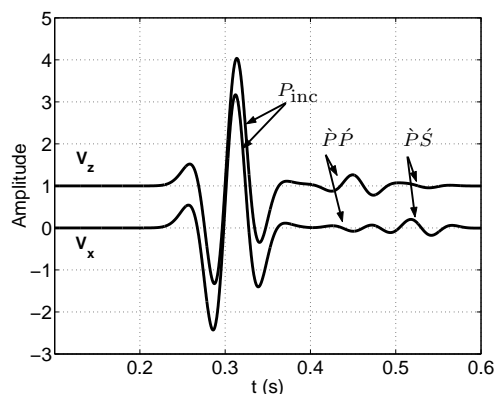


Fig. 4: Waveforms of PP and P-SV reflections: a) offset=0 m and b) offset=200 m. For offset=200 m, the lower trace is the  $x$ -component of the particle velocity,  $v_x$ , and the upper trace is the  $z$ -component of the particle velocity,  $v_z$ . Receivers are located at the depth of 1800 m.

- Schoenberg, M., 1980, Elastic wave behavior across linear slip interfaces: *J. Acoust. Soc. Am.*, **68**, 1516–1521.
- Schoenberg, M., 1998, Acoustic characterization of underground fractures: *Ann. Internat. Mtg., Soc. Expl. Geophys.*, Expanded Abstracts.
- Virieux, J., 1984, SH-wave propagation in heterogeneous media: Velocity-stress finite-difference method: *Geophysics*, **49**, 1933–1957.
- Virieux, J., 1986, P-SV wave propagation in heterogeneous media: Velocity-stress finite-difference method: *Geophysics*, **51**, 889–901.